Mechanics of Materials 130 (2019) 9–19

Contents lists available at ScienceDirect

Mechanics of Materials

journal homepage: www.elsevier.com/locate/mechmat

Thermomechanical constitutive modeling of fiber reinforced shape memory polymer composites based on thermodynamics with internal state variables

Jianping Gu[a,b], Jinsong Leng[c,*], Huiyu Sun[b,*], Hao Zeng[b], Zhongbing Cai[d]

[a] Jiangsu Key Laboratory of Advanced Structural Materials and Application Technology, School of Materials Science and Engineering, Nanjing Institute of Technology, Nanjing 211167, China
[b] State Key Laboratory of Mechanics and Control of Mechanical Structures, Nanjing University of Aeronautics and Astronautics, Nanjing 210016, China
[c] Center for Composite Materials and Structures, Harbin Institute of Technology, Harbin 150080, China
[d] Civil Engineering Department, Yancheng Institute of Technology, Yancheng 224051, China

ARTICLE INFO

Keywords:
Shape memory polymer composites
Unidirectional continuous fiber network
Finite deformation
Thermodynamics
Constitutive model

ABSTRACT

Shape memory polymer composites (SMPCs) can be used to improve the mechanical properties of the shape memory polymers (SMPs). They also have the potential to enhance or enable new stimulus approaches and novel shape memory effects (SMEs). In this paper, a thermoviscoelastic finite deformation constitutive model is developed for thermally activated unidirectional continuous elastic fiber reinforced SMPCs. Since the structural relaxation and viscous flow mainly exist in the SMP matrix, an internal state variable modeling approach is used to describe the thermomechanical behavior of the SMPCs. Recent works mainly focus on the thermomechanical behavior of carbon fiber reinforced SMPCs in the small strain range, for the tensile tolerant strain of carbon fiber is small. The model that is developed here shows that the unidirectional continuous carbon fiber reinforced SMPCs with proper fiber inclination angle and volume fraction can also be used in finite deformation range for the first time. The finite deformation thermomechanical response of unidirectional continuous carbon fiber reinforced SMPCs with different inclination angles and volume fractions is addressed here. Therefore, this study provides useful guidance for reasonable design of unidirectional continuous elastic fiber reinforced SMPCs.

1. Introduction

Shape memory polymers (SMPs) have drawn plenty of attention from all over the world for their capability to recover the initial shape even under the condition of large deformation. To date, many kinds of external stimuli have been developed to trigger the shape memory effects (SMEs) of SMPs, such as temperature, electricity, moisture or radiation (Li and Wang, 2016; Liu et al., 2009). There are so many advantages of SMPs compared with the shape memory metallic alloys (SMAs), such as light weight, low cost, large deformation, good biocompatibility and biodegradability. The potential application of SMPs is very broad, ranging from clothing manufacturing, intelligent medical equipments to self-deployable structures in aeronautics and astronautics (Leng et al., 2011).

The evident shortcoming of SMPs is that the mechanical properties of these materials are relatively low, which seriously limits the development in this area. Therefore, a number of shape memory polymer composites (SMPCs) have been developed to increase the mechanical properties of the SMP matrix. Besides, some of them also have the ability to enhance or enable new stimulus approaches and novel SMEs. Generally, SMPCs can be classified into two categories: fiber reinforced SMPCs and particle reinforced SMPCs. The SMPCs with long thin fibers have many outstanding mechanical properties, such as high stiffness and strength. Therefore, a larger recovery stress can be generated by the fiber reinforced SMPCs during the process of deformation recovery. Obviously, this is a desirable feature in engineering applications.

It is clear that the constitutive models are critical to analyze and predict the shape memory behaviors of SMPs and SMPCs. However, the modeling efforts lag far behind the achievements in developing novel SMPs and SMPCs. So far the modeling approaches for thermally activated SMPs can be classified into the phase transition modeling approaches and thermoviscoelastic modeling approaches. In the phase transition modeling approaches, the substance could be divided into two or more phases. Hence, the mechanism of shape memory behaviors can be explained by the transition between different phases. Generally, the approaches are used in modeling crystallizable polymers (Lu et al., 2016; Bouaziz et al., 2017). Liu et al. (2006) firstly used the phase transition approaches for amorphous SMPs on the assumption that the

* Corresponding authors.
E-mail addresses: lengjs@hit.edu.cn (J. Leng), hysun@nuaa.edu.cn (H. Sun).

https://doi.org/10.1016/j.mechmat.2019.01.004
Received 19 April 2018; Received in revised form 8 January 2019
Available online 09 January 2019
0167-6636/

substance can be divided into frozen phase and active phase. Though the phase transition modeling approaches are not physics-based description for amorphous SMPs, their phenomenological representations provide useful predictive tools (Boatti et al., 2016; Li et al., 2017). Recently, the modeling approaches are developing towards more physical descriptions of the underlying shape memory mechanisms. Diani et al. (2006) firstly proposed the 3D finite deformation thermo-viscoelastic model. The model can be used to describe the entropy elasticity of the high temperature response for amorphous polymers. Besides, the time-dependent and temperature-dependent viscoelastic behavior of the glass transition are addressed. Thereafter, the theoretical framework of Diani et al. (2006) was further developed by Nguyen et al. (2008), and a model incorporates structural relaxation and stress relaxation was proposed. In order to describe the multitude of relaxation processes, Xiao et al. (2013) amended the model by incorporating the multiple discrete structural and stress relaxation processes. Similar multi-branch modeling approaches were also used by Westbrook et al. (2011).

The fictive temperature θ_f can be used as an internal variable to describe the nonequilibrium structure during the glass transition of amorphous SMPs (Nguyen et al., 2008; Xiao et al., 2013). It should be noted that the fictive temperature approach was firstly introduced by Tool (1946) to model the structural relaxation in glasses. The relaxation time is one of the critical factors in describing the thermomechanical behavior of the material. Generally, the relaxation time model described by the fictive temperature is temperature dependent only. In the work of Gu et al. (2017), an internal state variable modeling approach developed by Lion et al. (2010) based on thermodynamics was used instead of the traditional phenomenological fictive temperature. The main reason is that the model of Lion et al. (2010) can extend the classical theories based on fictive temperature in two ways. Firstly, temperature effects and mechanical loadings are accounted for in a single consistent approach. Secondly, the basic thermodynamic potential is determined by the temperature, the stress and a set of internal variables.

Evidently, the constitutive models for thermally activated fiber reinforced SMPCs are more complicated to establish. By using the micromechanical method, Jarali et al., (2011) proposed a modeling approach for the effective properties and thermomechanical behavior of the SMA fiber reinforced SMPC laminates. In their study, the constitutive model of the SMP matrix is the same as the phase transition model developed by Liu et al. (2006), which is only applicable to the condition of small strain. In the work of Song et al. (2015), a linear constitutive model for the SMA fiber reinforced SMPC was developed based on the self-consistent homogenization approach. It should be noted that the constitutive model of the SMP matrix is also the same as the model developed by Liu et al. (2006). Therefore, the viscoelastic behavior of the SMP matrix is not taken into account in their work. Mao et al. (2015) studied the thermoviscoplastic behavior of a cold-programmed anisotropic shape memory elastomeric composite (SMEC) which is consisted of an elastomeric matrix reinforced by aligned amorphous polymer fibers. A 3D anisotropic thermoviscoelastic constitutive model was developed in their work to capture the cold-programmed SMEs and the dramatic non-affine shape change of the composite. By taking advantage of 3D printing, Ge et al. (2016) presented a new approach for fabricating printed anisotropic SMECs. The SMEs of the composites is triggered by the crystallizable polymeric fibers implanted in the matrix. To describe the complex, anisotropic, larger deformation thermomechanical behaviors of the composites, a constitutive model was developed in their work by incorporating the phase evolution theory for soft active materials into the existing theory for fiber reinforced hyperelastic composites.

It should be noted that carbon fibers are often used as the reinforcement phase in the SMP matrix, for its outstanding mechanical properties. Nishikawa et al. (2012) conducted periodic-cell simulations of the thermomechanical cycle for the discontinuous carbon fiber reinforced SMPC. In their work, the thermomechanical behavior of the SMP matrix was described by the liner constitutive model. Besides, the effects of fiber volume fraction, fiber aspect ratio and fiber end position on the shape fixity and shape recovery of the composite were studied in detail. Based on the bridging model, Tan et al. (2014) developed a constitutive model for axial unidirectional continuous carbon fiber reinforced SMPCs under thermomechanical loadings in the small strain range. The phase transition model proposed by Liu et al. (2006) was also used in their study for the SMP matrix. It should be noted that the recent works mainly focus on the thermomechanical behavior of carbon fiber reinforced SMPCs in small strain range, for the failure tensile strain of carbon fiber is small (about 2%). In this paper, the model developed here shows that the unidirectional continuous carbon fiber reinforced SMPCs with proper fiber inclination angle and volume fraction can also be used in finite deformation range for the first time.

This paper is arranged in the following order. The fundamental equations of the finite deformation constitutive model for the unidirectional continuous fiber reinforced SMPCs are shown in Section 2. The approach for the determination of model parameters is briefly introduced in Section 3. Then the model prediction of the thermomechanical behavior and the SMEs of the composites are adequately presented in this section. Reviews and future work are discussed in Section 4.

2. Constitutive model

A finite deformation constitutive model of fiber reinforced SMPCs is presented in this section by using the approach proposed by Gu et al. (2017), based on thermodynamics with internal state variables. The stress-strain response of the fiber is regarded as linearity. The mechanical properties of the SMPCs is determined by mesomechanics. Fig. 1 illustrates the stress-deformation response of the model for fiber reinforced SMPCs.

2.1. Structural relaxation

As demonstrated previously, the approach proposed by Lion et al. (2010) has the advantages of good applicability and more definite physics-based description, compared to the fictive temperature approach. In the work of Gu et al. (2017), it is demonstrated that the approach is rather effective in describing the structural relaxation of the amorphous SMPs in the glass transition. Since the structural relaxation mainly exists in the SMP matrix, it is assumed that the approach is still valid in modeling the structural relaxation of elastic fiber reinforced SMPCs.

In the model of Lion et al. (2010), the vicinity of the thermodynamic equilibrium reference state is described by the sufficient small fluctuations of the variables (stress tensor $\boldsymbol{T}$, strain tensor $\boldsymbol{E}$, temperature θ,

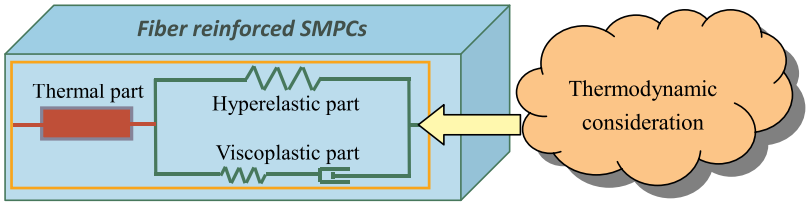

Fig. 1. 1D analogy of the constitutive model for the fiber reinforced SMPCs.

specific entropy s per unit mass and internal variable tensor $\boldsymbol{\alpha}$). The internal variable $\boldsymbol{\alpha}$ is used to describe the history-dependent properties of thermoviscoelastic materials in the vicinity of the glass transition. It can be determined by a system of ordinary differential equations depending on the selected set of external variables ($\boldsymbol{E}$, s), ($\boldsymbol{T}$, s), ($\boldsymbol{E}$, θ) or ($\boldsymbol{T}$, θ) and the current value of the internal variable itself (Lion et al., 2010). Therefore, the values of the variables in the current state can be obtained by

$$\boldsymbol{T} = \boldsymbol{T}_{ref} + \boldsymbol{\Sigma}(t) \tag{1a}$$

$$\boldsymbol{E} = \boldsymbol{E}_{ref} + \boldsymbol{\Gamma}(t) \tag{1b}$$

$$\theta = \theta_{ref} + \vartheta(t) \tag{1c}$$

$$s = s_{ref} + \eta(t) \tag{1d}$$

$$\alpha = \alpha_{ref} + \delta(t) \tag{1e}$$

where $\boldsymbol{T}_{\mathrm{ref}}$, $\boldsymbol{E}_{\mathrm{ref}}$, θ_{ref}, s_{ref} and $\boldsymbol{\alpha}_{\mathrm{ref}}$ are reference values in an equilibrium reference state, $\Sigma(t)$, $\Gamma(t)$, $\vartheta(t)$, $\eta(t)$ and $\boldsymbol{\delta}(t)$ are perturbation functions.

For simplicity, the tensors in Eq. (1) can be written in Voigt notation, e.g.

$$\boldsymbol{T} = \begin{bmatrix} T_{11} & T_{12} & T_{13} \\ T_{21} & T_{22} & T_{23} \\ T_{31} & T_{31} & T_{33} \end{bmatrix} \rightarrow \{\boldsymbol{T}\} = [T_{11} \quad T_{22} \quad T_{33} \quad T_{12} \quad T_{23} \quad T_{13}]^{\mathrm{T}} \tag{2}$$

where the subscripts 1, 2 and 3 denote the normal directions. Deduced from the Clausius–Duhem inequality, the correlations of the perturbations are given by Lion et al. (2010) as follows:

$$\{\Gamma\} = \boldsymbol{D}_0\{\Sigma\} + k_0\vartheta - \rho\boldsymbol{w}\{\delta\} \tag{3a}$$

$$\eta = \frac{c_{p0}}{\theta_{ref}}\vartheta - e\cdot\{\delta\} + \frac{1}{\rho}k_0\cdot\{\Sigma\} \tag{3b}$$

$$\{\dot{\delta}\} = -\frac{1}{\tau}\left(\{\delta\} + \frac{e}{d}\vartheta + \frac{w^T}{d}\{\Sigma\}\right) \tag{3c}$$

where c_{p0}, ρ and d are specific heat, density and material parameter, respectively. $\boldsymbol{k}_0$, $\boldsymbol{e}$ are the parameter vectors which can be represented as:

$$\boldsymbol{k}_0 = [k_0 \quad k_0 \quad k_0 \quad 0 \quad 0 \quad 0]^T \tag{4}$$

$$\boldsymbol{e} = [e \quad e \quad e \quad 0 \quad 0 \quad 0]^T \tag{5}$$

where k_0 is the thermal expansion coefficient and e is the parameter which can be used to describe the coupling between the temperature and the internal variables. $\boldsymbol{D}_0$ is the compliance of the glassy state material which can be expressed as

$$\boldsymbol{D}_0 = \frac{1}{E}\begin{bmatrix} 1 & -\mu & -\mu & 0 & 0 & 0 \\ -\mu & 1 & -\mu & 0 & 0 & 0 \\ -\mu & -\mu & 1 & 0 & 0 & 0 \\ 0 & 0 & 0 & 2(1+\mu) & 0 & 0 \\ 0 & 0 & 0 & 0 & 2(1+\mu) & 0 \\ 0 & 0 & 0 & 0 & 0 & 2(1+\mu) \end{bmatrix} \tag{6}$$

where E is the Young's modulus and μ is the Poisson's ratio. $\boldsymbol{w}$ can be used to describe the coupling between the stress and the internal variables.

$$\boldsymbol{w} = \begin{bmatrix} w_t & v_t & v_t & 0 & 0 & 0 \\ v_t & w_t & v_t & 0 & 0 & 0 \\ v_t & v_t & w_t & 0 & 0 & 0 \\ 0 & 0 & 0 & w_s & 0 & 0 \\ 0 & 0 & 0 & 0 & w_s & 0 \\ 0 & 0 & 0 & 0 & 0 & w_s \end{bmatrix} \tag{7}$$

where w_t, v_t and w_s are the additional material parameters. τ is the structural relaxation time that can be written as

$$\tau = \tau_0 \exp\left(\frac{B}{\theta s}\right) \tag{8}$$

where B is the activation parameter.

2.2. Deformations and stresses

The deformation of a 3D solid body is described by the deformation gradient $\boldsymbol{F}$ which can be used to determine the deformation from its reference configuration Ω_0 in thermodynamic equilibrium to the current configuration Ω. Here, it is assumed that the general thermo-mechanical deformation of the SMPCs can be firstly split locally into two parts.

$$\boldsymbol{F} = \boldsymbol{F}^M\boldsymbol{F}^\theta \tag{9}$$

where $\boldsymbol{F}^{\mathrm{M}}$ and $\boldsymbol{F}^{\theta}$ are the mechanical and thermal deformations, respectively. $\boldsymbol{F}^{\mathrm{M}}$ can further be separated into elastic and viscous parts as follows:

$$\boldsymbol{F}^M = \boldsymbol{F}^e\boldsymbol{F}^v \tag{10}$$

where $\boldsymbol{F}^{v}$ is a relaxed configuration obtained by elastically unloading $(\boldsymbol{F}^e)^{-1}$.

As shown in Fig. 1, the mechanical behavior of the SMPCs can be decomposed into two parts: an equilibrium response and a time-dependent deviation from equilibrium. Therefore, it is appropriate to split the general stress into an equilibrium part σ^n and a nonequilibrium time-dependent part $\sigma^v(\sigma^e)$ representing the viscoplastic behavior.

The stress of the equilibrium component can be obtained by using the hyperelastic constitutive model for fiber reinforced composites of Guo et al. (2007). The model for the transversely isotropic material is developed based on a multiplicative decomposition of the deformation gradient (a uniaxial deformation along the fiber direction and a subsequent shear deformation) which considers interaction between the fiber and the matrix. In the model of Guo et al. (2007), the Cauchy stress of the transversely isotropic fiber reinforced hyperelastic composites can be written as

$$\sigma^n = -p\boldsymbol{I} + G_c\boldsymbol{F}^M(\boldsymbol{F}^M)^T + cG_c(1 - I_4^{-3/2})\boldsymbol{F}^M\boldsymbol{a}_0 \otimes \boldsymbol{F}^M\boldsymbol{a}_0 \tag{11}$$

where $\boldsymbol{I}$ is the second order identity tensor, p is an arbitrary hydrostatic pressure, G_{c} is an effective shear modulus of the composite. Parameters c can be expressed as

$$c = (G_{\mathrm{m}}v_{\mathrm{m}} + G_{\mathrm{f}}v_{\mathrm{f}} - G_{\mathrm{c}})/G_{\mathrm{c}} \tag{12}$$

where G_{m} and G_{f} are the shear moduli of the matrix and fiber, v_{m} and v_{f} are the volume fractions of the matrix and fiber. $\boldsymbol{a}_0$ is the fiber direction in the reference configuration in the composite. Therefore, $\boldsymbol{F}^{\mathrm{M}}\boldsymbol{a}_0$ can be used to represent the fiber direction in the current configuration. The additional invariant I_4 can be given by

$$I_4 = \boldsymbol{F}^M a_0\cdot\boldsymbol{F}^M a_0 \tag{13}$$

It is also known that $\lambda_f = \sqrt{I_4}$ is the stretch in the fiber direction.

As Fig. 1 shows, the stress of the nonequilibrium part caused by the viscous deformation can be derived through F^{e} as follows:

$$\sigma^v = \sigma^e = \frac{1}{J^e}\boldsymbol{L}^e\colon\boldsymbol{E}^e \tag{14}$$

where $J^{\mathrm{e}} = \det(\boldsymbol{F}^{\mathrm{e}})$, $\boldsymbol{E}^{\mathrm{e}} = \boldsymbol{V}^{\mathrm{e}} - \boldsymbol{I}$, and $\boldsymbol{L}^{\mathrm{e}}$ is the fourth order elasticity tensor.

Therefore, the total stress acting on the system can be obtained as

$$\boldsymbol{\sigma} = \boldsymbol{\sigma}^{\mathrm{n}} + \boldsymbol{\sigma}^{\mathrm{e}} \tag{15}$$

2.3. The viscous flow rule

As demonstrated previously, the viscoplastic stretch rate $\boldsymbol{D}_{\mathrm{v}}$ can be constitutively described by the plastic shear strain rate $\dot{\gamma}_V$ though

$$\boldsymbol{D}_V = \dot{\gamma}_V\boldsymbol{n} \tag{16}$$

where $\boldsymbol{n}=\boldsymbol{\sigma}'_v/\|\boldsymbol{\sigma}'_v\|$ is the direction of the flow stress and $\boldsymbol{\sigma}'_v = \boldsymbol{\sigma}_v - 1/3\mathrm{tr}(\boldsymbol{\sigma}_v)\boldsymbol{I}$ is the deviatoric part of $\boldsymbol{\sigma}_v$.

Generally, the Eyring model is applied to describe the temperature-dependent, stress-activated property of viscoplastic flow for the glassy state polymers. In the work of Gu et al. (2017), a modified Eyring model incorporated with Eq. (8) is developed to extend the viscoplastic flow rule to the glass transition and the vicinity of the process.

$$\dot{\gamma}_V = \frac{s_y}{\eta_{\mathrm{ref}}}\frac{\theta}{Q}\exp\left(\frac{-B}{\theta s}\right)\sinh\left(\frac{Q}{\theta}\frac{\bar{\tau}}{s_y}\right) \tag{17}$$

where s_y is the athermal shear strength, η_{ref} is the reference shear viscosity, Q is the activation parameter, and $\bar{\tau} = \|\sigma'_v\|/\sqrt{2}$ is the equivalent shear stress.

2.4. Thermal deformation

Here, a coefficient of thermal expansion (CTE) model for the transversely isotropic composite is developed by assuming that the fiber reinforced SMPCs are two phases homogenized systems. It is considered that the SMPCs can be divided into SMP phase and fiber phase. Based on the method of mesomechanics, the longitudinal CTE of the axial unidirectional continuous fiber reinforced SMPCs can be derived as

$$\alpha_1 = \frac{\alpha_m E_m v_m + \alpha_{f1} E_{f1} v_f}{E_m v_m + E_{f1} v_f} \tag{18}$$

where α_m and α_{f1} are the equivalent CTE of the isotropic SMP matrix and longitudinal CTE of the fiber, E_m and E_{f1} are the Young's moduli of the SMP matrix and longitudinal Young's moduli of the fiber. Here, the CTE of the fiber is regarded as temperature-independent. Since the CTE of the SMP matrix is temperature-dependent in the range of glass transition, the equivalent CTE of SMP is defined as

$$\alpha_m = \frac{\varepsilon_{m,\theta}}{\theta - \theta_0} \tag{19}$$

where θ and θ_0 are the current temperature and initial temperature, respectively. $\varepsilon_{m,\theta}$ is the thermal strain of the SMP, which can be derived from Eq. (3a), under the condition of $\{\Sigma\} = \{0\}$. By using the rule of mixture, the transverse CTE of the SMPCs can be obtained as

$$\alpha_2 = \alpha_m(1+\mu_m)v_m + \alpha_{f2}(1+\mu_f)v_f - \alpha_1\mu_{21} \tag{20a}$$

$$\mu_{21} = (\mu_m v_m + \mu_f v_f) \tag{20b}$$

where α_{f2} is the transverse CTE of the fiber, μ_m and μ_f are the Poisson's ratios of the SMP matrix and fiber.

As shown in Fig. 2, the CTEs of the SMPCs in x-y plane can be calculated as follows, through the coordinate transformation formula.

$$\alpha_x = \alpha_1\cos^2\varphi + \alpha_2 sin^2\varphi \tag{21a}$$

$$\alpha_y = \alpha_1 sin^2\varphi + \alpha_2\cos^2\varphi \tag{21b}$$

$$\alpha_{xy} = 2(\alpha_1 - \alpha_2)sin\varphi\cos\varphi \tag{21c}$$

where φ is the inclination angle of the fiber, which is also defined as the angle rotated on the x-axis. It should be noted that the CTE of the SMPCs in the z direction is not affected by the inclination angle of the fiber, and always equals to α_2.

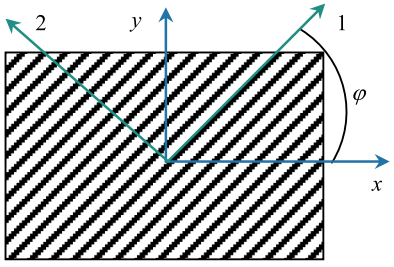

Fig. 2. Relations of coordinate systems of a fiber reinforced SMPCs.

During a thermomechanical shape memory cycle, the transversely isotropic SMPCs have thermal deformation gradients in the following form:

$$\boldsymbol{F}^T = \begin{bmatrix} \lambda_{xx}^{\mathrm{T}} & S_{xy}^{\mathrm{T}} & 0 \\ 0 & \lambda_{yy}^{\mathrm{T}} & 0 \\ 0 & 0 & \lambda_{zz}^{\mathrm{T}} \end{bmatrix} \tag{22}$$

where S_{xy}^{T} is the thermal shear strain and equals to $\alpha_{xy}(\theta - \theta_0)$. The normal components can be written as

$$\lambda_{ii}^{\mathrm{T}} = 1 + \varepsilon_{ii}^{\mathrm{T}} (i = x, y, z) \tag{23}$$

where $\varepsilon_{ii}^{\mathrm{T}}$ is the thermal strain in normal direction and equals to $\alpha_{ii}(\theta - \theta_0)$.

3. Results and discussions

The thermomechanical behavior of unidirectional continuous carbon fiber reinforced SMPCs has been studied in the earlier sections. In the simulations to follow, the SMP matrix is an acrylate-based network polymer. The reinforcement material is T700 Toray carbon fiber. It is assumed that the fibers are uniformly distributed throughout the matrix. Therefore, the SMPC studied here is an ideal transversely isotropic material.

3.1. Determination of model parameters

A series of tests were carried out by Westbrook et al. (2011) to determine the material properties of the SMP. Model parameters related to the SMP matrix listed in Table 1 can either be measured from or fitted to the experimental data (Gu et al., 2017). The parameters of the carbon fiber are listed in Table 2.

Mahieux and Reifsnider (2001) presented a temperature-dependent model for the storage modulus E' of the polymers at a constant frequency as follows:

$$E'(\theta) = (E'_1 - E'_2)\cdot\exp\left(-\left(\frac{\theta}{\theta_\beta}\right)^{m_1}\right) + (E'_2 - E'_3)\cdot\exp\left(-\left(\frac{\theta}{\theta_g}\right)^{m_2}\right) + E'_3\cdot\exp\left(-\left(\frac{\theta}{\theta_f}\right)^{m_3}\right) \tag{24}$$

where θ_β, θ_g and θ_f are the temperatures of β-transition, glass transition and beginning of the flow region, respectively. E'_i and m_i $(i = 1, 2, 3)$ are the instantaneous stiffness at the beginning of each transition and Weibull exponents corresponding to the statistics of the bond breakage. As shown in Fig. 3, the values of the parameters above can be determined by fitting the Dynamic Mechanical Analysis (DMA) experiment.

Generally, it is considered that the Young's modulus E_m of the SMPs is equal to the storage modulus E' since the loss modulus is usually much less than the storage modulus. In the paper, the phase transition approach is used to describe the temperature dependence of Poisson's ratio μ_m of the SMP matrix (Qi et al., 2008).

$$\mu_m = \mu_g f_g + \mu_r(1 - f_g) \tag{25a}$$

$$f_g = 1 - \frac{1}{1 + \exp[-(\theta - \theta_m)/Z]} \tag{25b}$$

where μ_g and μ_r are the Poisson's ratios of the frozen phase and active phase, respectively. f_g is the volume fraction of the frozen phase. θ_m and Z are the reference temperature and the parameter related to the width of the phase transition zone, respectively. As detailed in Gu et al. (2017), other parameters listed in Table 1 can be obtained by fitting of the thermal strain of the SMP matrix.

Table 1
Parameters of the model for the SMP matrix.

Parameters	Values
θ_β (β-transition temperature)	22.2 °C
θ_g (Glass transition temperature)	32 °C
θ_f (Temperature at the beginning of the flow region)	142.5 °C
E'_1 (Material stiffness at the beginning of β-transition)	2552.9 MPa
E'_2 (Material stiffness at the beginning of glass transition)	1876.3 MPa
E'_3 (Material stiffness at the beginning of flow region)	5 MPa
m_1, m_2, m_3 (Weibull exponents)	19.3, 58.4, 177.6
μ_g (Poisson's ratio of the frozen phase)	0.35
μ_r (Poisson's ratio of the active phase)	0.499
θ_m (Reference temperature for phase transition)	27.5 °C
Z (Parameter characterizing the width of the phase transition zone)	7
Q/s_y (Activation parameter for viscous flow)	175 °C/MPa
η_{ref} (Reference shear viscosity)	12 MPa s
θ_{ref} (Temperature of thermodynamic equilibrium reference state)	25 °C
s_{ref} (Specific entropy of thermodynamic equilibrium reference state)	6 J/kg K
T_{1ref} (Uniaxial stress of thermodynamic equilibrium reference state)	−5 MPa
c_{p0} (Specific heat)	50 J/kg K
k_0 (Thermal expansion coefficient)	1.4×10^{-4} /°C
d (Parameter for internal variable perturbations)	1.5×10^{-17} J/kg
e, w_t, v_t (Parameter for influence of coupling)	1.5×10^{-9} J/kg K, 1×10^{-16} m^3/kg, 5×10^{-16} m^3/kg
B (Activation parameter for structural relaxation)	20,000 J/kg
τ_{R0} (Reference value of structural relaxation time)	3×10^{-2} s
ρ (Density of the material)	1050 kg/m^3

Table 2
Material parameters of the carbon fiber.

Parameters	Values
E_{f1} (Longitudinal Young's modulus)	230 GPa
E_{f2} (Transverse Young's modulus)	8.2 GPa
G_{f12} (Shear modulus in 1–2 plane)	27.3 GPa
μ_f (Poisson's ratio)	0.25
α_{f1} (Longitudinal coefficient of thermal expansion)	-8.3×10^{-7} /°C
α_{f2} (Transverse coefficient of thermal expansion)	10×10^{-6} /°C
C (Transverse contact coefficient between fibers)	0.2

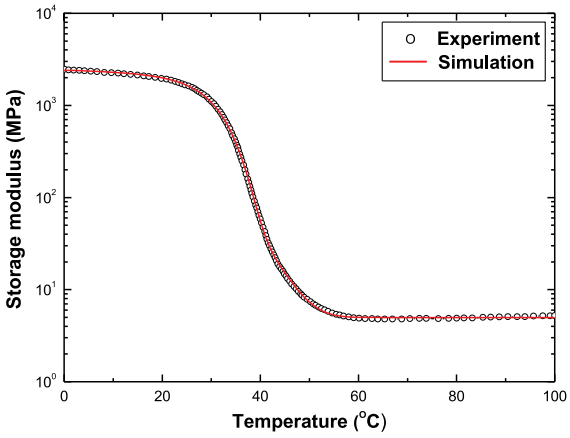

Fig. 3. Temperature-dependent parameter fitting for storage modulus.

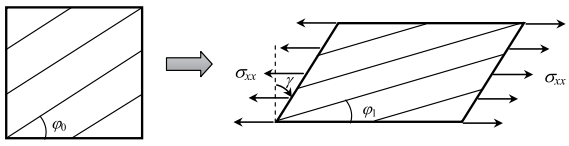

Fig. 4. Cartoon illustrating the loading applied onto the SMPC lamina.

Under the assumption that the fibers and the matrix have the same deformation in the fiber direction, the effective elastic constants of the transversely isotropic SMPCs can be determined as follows, based on the theory of volume averaging (Shen and Hu, 2006).

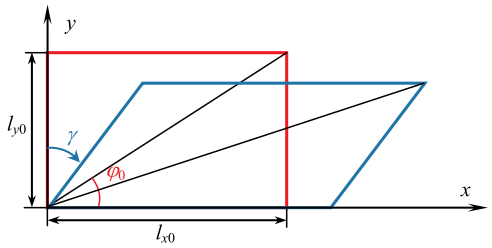

Fig. 5. Geometry of the representative element of deformation.

$$E_{C1} = E_{f1}v_f + E_m v_m \tag{26a}$$

$$E_{C2} = (1 - C)E^1_{C2} + CE^2_{C2} \tag{26b}$$

$$\mu_{C21} = (1 - C)\mu^1_{C21} + C\mu^2_{C21} \tag{26c}$$

$$\mu_{C12} = \mu_{C21}\frac{E_{C2}}{E_{C1}} \tag{26d}$$

$$G_{C12} = (1 - C)G^1_{C12} + CG^2_{C12} \tag{26e}$$

where C is the transverse contact coefficient between the fibers. Superscripts 1 and 2 denote the constants associated with models, respectively, in series and in parallel.

$$E^1_{C2} = \frac{E_{f2}E_m}{E_{f2}v_m + E_m v_f} \tag{27a}$$

$$E^2_{C2} = E_{f2}v_f + E_m v_m \tag{27b}$$

$$\mu^1_{C21} = \mu_f v_f + \mu_m v_m \tag{27c}$$

$$\mu^2_{C21} = \frac{\mu_f E_{f2} v_f + \mu_m E_m v_m}{E_{f2}v_f + E_m v_m} \tag{27d}$$

$$G^1_{C12} = \frac{G_{f12}G_m}{G_{f12}v_m + G_m v_f} \tag{27e}$$

$$G^2_{C12} = G_{f12}v_f + G_m v_m \tag{27f}$$

It should be noted that the values of the effective elastic constants are between the values calculated by series model and the values

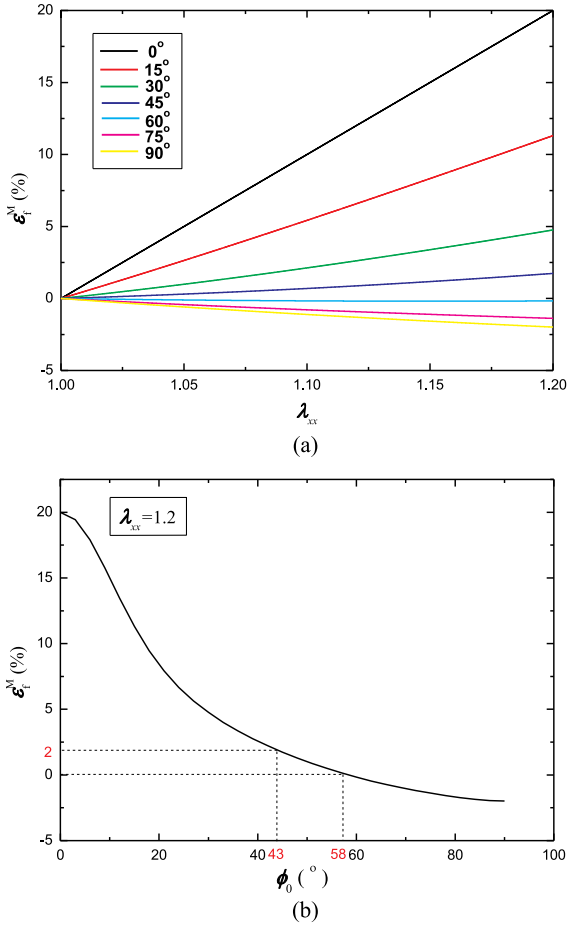

Fig. 6. Variation of the mechanical tensile strain of the carbon fibers with different initial inclination angles in response to x direction stretch.

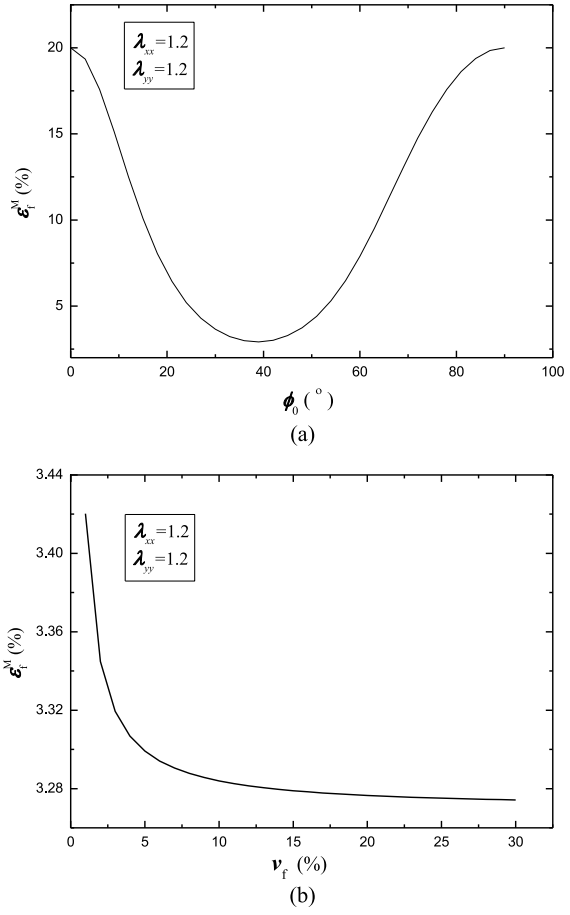

Fig. 7. Variation of the mechanical tensile strain of the carbon fiber in response to the fiber inclination angle and fiber volume fraction under biaxial tension.

calculated by parallel model. It has been demonstrated that the model is valid in calculating the effective elastic constants for glass fiber/epoxy composites. The comparison with the experimental data indicates that the empirical value of C for the glass fiber/epoxy composites is 0.2 (Shen and Hu, 2006). Due to the reason that both the glass fiber/epoxy composites and the carbon fiber reinforced SMPCs are elastic fiber reinforced polymer composites, the model is also adopted in our study. For simplicity, the value of C is also equal to 0.2 in our study since the objective of our work is providing guidance for reasonable design of the elastic fiber reinforced SMPCs in theory.

In the condition of plane stress, the relation of stress and strain can be written as

$$\begin{bmatrix} \sigma_{xx} \\ \sigma_{yy} \\ \tau_{xy} \end{bmatrix} = \bar{Q} \begin{bmatrix} \varepsilon_{xx} \\ \varepsilon_{yy} \\ \gamma_{xy} \end{bmatrix} \tag{28}$$

where constitutive matrix $\bar{Q}$ can be obtained by

$$\bar{Q} = T^{-1} Q (T^{-1})^{\mathrm{T}} \tag{29}$$

where T is the coordinate transformation matrix for the x-y coordinate system that can be given by

$$T = \begin{bmatrix} \cos^2\varphi & sin^2\varphi & 2\sin\varphi\cos\varphi \\ sin^2\varphi & \cos^2\varphi & -2\sin\varphi\cos\varphi \\ -\sin\varphi\cos\varphi & \sin\varphi\cos\varphi & \cos^2\varphi - sin^2\varphi \end{bmatrix} \tag{30}$$

where φ denotes the angle rotated on the x-axis, as shown in Fig. 2. Constitutive matrix Q can be written as

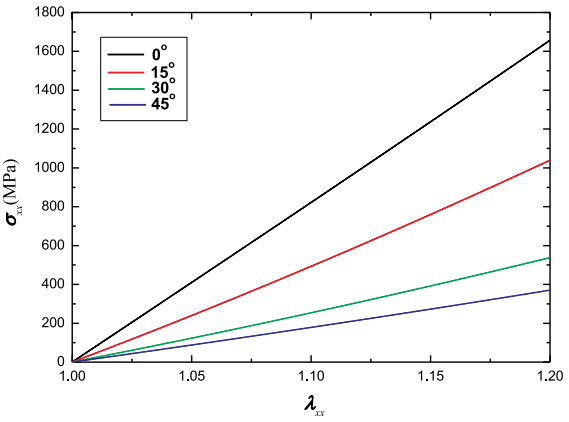

Fig. 8. Variation of x direction stress of the SMPCs with different inclination angles in response to x direction stretch.

$$Q = \begin{bmatrix} Q_{11} & Q_{12} & 0 \\ Q_{12} & Q_{22} & 0 \\ 0 & 0 & Q_{66} \end{bmatrix} \tag{31}$$

where $Q_{11} = E_{C1}/(1-\mu_{C12}\mu_{C21})$, $Q_{22} = E_{C2}/(1-\mu_{C12}\mu_{C21})$, $Q_{12} = \mu_{C21}E_{C2}/(1-\mu_{C12}\mu_{C21})$ and $Q_{66} = G_{C12}$.

3.2. Model prediction

In this subsection, the simulations are carried out to predict the thermomechanical behavior of the unidirectional continuous carbon

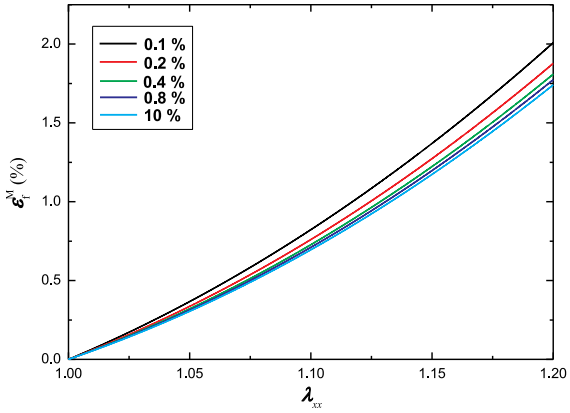

Fig. 9. Variation of the mechanical tensile strain of the carbon fibers with different fiber volume fractions in response to x direction stretch.

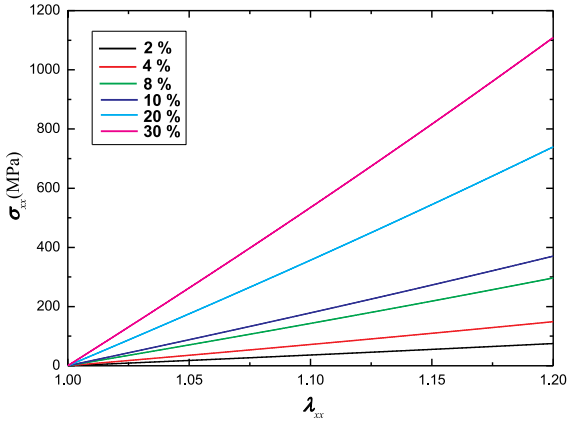

Fig. 10. Variation of x direction stress of the SMPCs with different fiber volume fractions in response to x direction stretch.

Table 3
Thermomechanical programming and recovery environment.

Step	Condition	Temperature
1. Loading (20% strain)	Strain rate 0.01 /s	60 °C
2. Holding	Cooling rate −2.5 °C/min	10 °C
3. Unloading	Strain rate −0.01 /s	10 °C
4. Heating	Heating rate 2.5 °C/min	60 °C

fiber reinforced SMPC lamina. It is considered that the SMPC lamina is in the state of plane stress and only a longitudinal stress is applied on the lamina, as illustrated in Fig. 4.

Generally, the total deformation gradient of the lamina during a shape memory cycle can be written as

$$\boldsymbol{F} = \begin{bmatrix} \lambda_{xx} & S_{xy} & 0 \\ 0 & \lambda_{yy} & 0 \\ 0 & 0 & \lambda_{zz} \end{bmatrix} \tag{32}$$

where S_{xy} is the total shear strain, λ_{ii} $(i = x, y, z)$ is the total stretch in i direction. Based on Eq. (9), the mechanical deformation gradient can be written as

$$F^{\mathrm{M}} = \begin{bmatrix} \lambda_{xx}^{\mathrm{M}} & S_{xy}^{\mathrm{M}} & 0 \\ 0 & \lambda_{yy}^{\mathrm{M}} & 0 \\ 0 & 0 & \lambda_{zz}^{\mathrm{M}} \end{bmatrix} \tag{33}$$

The mechanical deformation is regarded as incompressible, whence,

$$\lambda_{xx}^{\mathrm{M}}\lambda_{yy}^{\mathrm{M}}\lambda_{zz}^{\mathrm{M}} = 1 \tag{34}$$

The corresponding Cauchy stress tensor σn can be calculated from Eq. (11) as follows:

$$\boldsymbol{\sigma}^{\mathrm{n}} = \begin{bmatrix} \sigma_{xx}^{n} & \tau_{xy}^{\mathrm{n}} & 0 \\ \tau_{yx}^{\mathrm{n}} & \sigma_{yy}^{n} & 0 \\ 0 & 0 & \sigma_{zz}^{n} \end{bmatrix} \tag{35}$$

It is clear that the boundary conditions are $\tau_{xy}^{\mathrm{n}} = \tau_{yx}^{\mathrm{n}} = 0$, $\sigma_{yy}^{n} = 0$ and $\sigma_{zz}^{n} = 0$ for the lamina in the state of plane stress and only σ_{xx} is applied on it. In a thermomechanical strain-controlled programming, the variation of λ_{xx} is definite. Therefore, the arbitrary hydrostatic pressure p and the mechanical deformation gradients of other directions can be derived from the boundary conditions. Finally, the value of σ_{xx}^{n} at any temperature and any time can be obtained from Eq. (11).

Generally, the recent works mainly focus on the thermomechanical SME of carbon fiber reinforced SMPCs in the small strain range, for the failure tensile strain of carbon fiber is very small (about 2%). As shown in Fig. 5, the total tensile strain of carbon fiber can be derived through the geometry of the representative element. Firstly, the initial length of the carbon fiber can be written as

$$l_{\mathrm{f}0} = \sqrt{l_{x0}^2 + l_{y0}^2} = l_{x0}\sqrt{1 + \tan^2\varphi_0} \tag{36}$$

where l_{x0} and l_{y0} are the initial width and height of the representative element, respectively. Clearly, the width and height of the representative element in the deformed shape can be calculated as $l_x = \lambda_{xx}l_{x0}$ and $l_y = \lambda_{yy}l_{y0}$, respectively. According to the law of cosines, the deformed length of the carbon fiber can be written as

$$l_{\mathrm{f}} = \sqrt{l_x^2 + (l_y/\cos\gamma)^2 - 2l_x(l_y/cos\gamma)\cos(\pi/2 + \gamma)} \tag{37}$$

where γ is the shear deformation. Since the total tensile strain of the carbon can be defined as of $\varepsilon_{\mathrm{f}} = l_{\mathrm{f}}/l_{\mathrm{f}0} - 1$, ε_{f} can be obtained by

$$\varepsilon_{\mathrm{f}} = \sqrt{\frac{\lambda_{xx}^2 + (\lambda_{yy}\tan\varphi_0/\cos\gamma)^2 - 2\lambda_{xx}\lambda_{yy}\tan\varphi_0\cos(\pi/2 + \gamma)/\cos\gamma}{1 + \tan^2\varphi_0}} - 1 \tag{38}$$

As the thermal deformation taken into account, the mechanical tensile strain of the carbon fiber can be given by

$$\varepsilon_{\mathrm{f}}^{\mathrm{M}} = \varepsilon_{\mathrm{f}} - \alpha_1\Delta\theta \tag{39}$$

where $\Delta\theta$ is the change of temperature. According to Eqs. (38) and (39), the inclination angle of the fiber can distinctly affect the mechanical tensile strain of the carbon fiber. Therefore, the variation of $\varepsilon_{\mathrm{f}}^{\mathrm{M}}$ of the SMPCs with fiber volume fraction $v_{\mathrm{f}} = 10\%$ and different inclination angles in response to λ_{xx} at 60 °C under uniaxial tension is depicted in Fig. 6. It can be seen from Fig. 6(a) that $\varepsilon_{\mathrm{f}}^{\mathrm{M}}$ of the SMPC with the inclination angle $\varphi_0 < 60^\circ$ increases as λ_{xx} increases. Clearly, the SMPC with a larger φ_0 has a smaller $\varepsilon_{\mathrm{f}}^{\mathrm{M}}$. It is found from Fig. 6(b) that the $\varepsilon_{\mathrm{f}}^{\mathrm{M}}$ of the SMPC with $43^\circ < \varphi_0 < 58^\circ$ is in the range of 0%~2% while the stretch of the SMPC is 1.2, which means the unidirectional continuous carbon fiber reinforced SMPC with the proper fiber inclination angle can be used even in the finite deformation. Therefore, the following study in the paper focuses on the finite deformation SMEs of these SMPCs. Similarly, it can be seen from Fig. 6(a) that $\varepsilon_{\mathrm{f}}^{\mathrm{M}}$ of the SMPC with $\varphi_0 \geq 60^\circ$ increases as λ_{xx} increases. It also should be noted that $\varepsilon_{\mathrm{f}}^{\mathrm{M}}$ of the SMPC with $\varphi_0 \geq 60^\circ$ is the compressive strain, although λ_{xx} of the SMPC is the tensile stretch. Since the carbon fiber will buckle under the compressive strain, the SMPCs with these inclination angles are not stable. Therefore, they will not be studied in the paper.

There are several biaxial loading methods in practice. The simplest one is equibiaxial load. Here, the variation of $\varepsilon_{\mathrm{f}}^{\mathrm{M}}$ of the SMPC with fiber volume fraction $v_{\mathrm{f}} = 10\%$ at 60 °C in response to the fiber inclination angle under equibiaxial tension is depicted in Fig. 7(a), in the condition of $\lambda_{xx} = \lambda_{yy} = 1.2$. It is shown that the $\varepsilon_{\mathrm{f}}^{\mathrm{M}}$ of the SMPC decreases as the

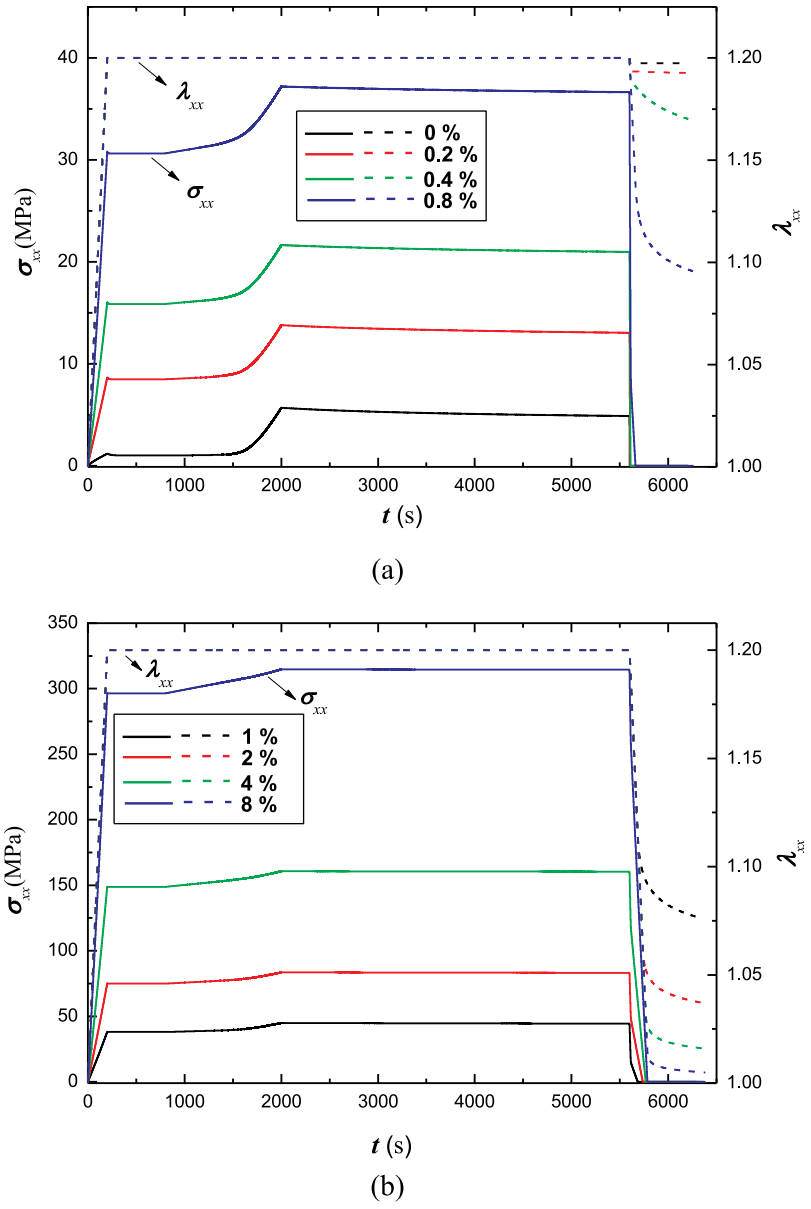

Fig. 11. Simulation results of SMPCs with different fiber volume fractions for stress and stretch separately as a function of time in the first 3 steps.

Table 4
Shape fixity ratios of the SMPCs with different fiber volume fractions.

v_f	0	0.2%	0.4%	0.8%	1%	2%	4%	8%
R_{fix}	98.7%	96.3%	85.1%	47.8%	38.5%	18.6%	8%	2%

φ_0 increases firstly. After reaching the minimum value, ε_f^M increases with the increasing of φ_0. It is calculated that the minimum value of ε_f^M is still above 2% which indicates that the carbon fiber will be invalid under this kind of biaxial loading regardless of the fiber inclination angle. The variation of ε_f^M of the SMPC with $\varphi_0 = 45^\circ$ at 60 °C in response to the fiber volume fraction under equibiaxial tension is depicted in Fig. 7(b). It can be found that the ε_f^M of the SMPC slightly decreases as the v_f increases and finally approaches a steady value which is still larger than 2%. Therefore, only the thermomechanical behavior of the SMPCs under uniaxial tension is studied in the following work.

Fig. 8 shows the stress σ_{xx} of the SMPCs with $v_f = 10\%$ and $\varphi_0 < 60^\circ$ in response to λ_{xx} at 60 °C without consideration of the fiber failure. Evidently, the stress of the SMPCs is greatly improved by the carbon fiber, which means the SMPCs may used in a broader application than SMPs. In addition, the carbon fiber with a smaller inclination angle can provide more reinforcement, which is also depicted in Fig. 8. Theoretically, the allowable tensile stretch of SMPCs with $\varphi_0 < 43^\circ$ could not reach the range of finite deformation. Therefore, it should be more effective to raise the fiber volume fraction v_f in improving the stiffness of the SMPCs than change the fiber inclination angle. Fig. 9 depicts the variation of ε_f^M of the SMPCs with $\varphi_0 = 45^\circ$ and different fiber volume fractions in response to λ_{xx} at 60 °C. It is found that the ε_f^M slightly decreases as v_f increases and become steady finally. The ε_f^M of SMPCs with $v_f \geq 0.2\%$ is less than 2% while the stretch of the SMPC is 1.2. Therefore, it can be concluded that the unidirectional continuous carbon fiber reinforced SMPC with $v_f \geq 0.2\%$ and $\varphi_0 = 45^\circ$ can be reliably used in the condition that $\lambda_{xx} \leq 1.2$. Fig. 10 shows the influences of v_f on the mechanical properties of the SMPCs with $\varphi_0 = 45^\circ$. Clearly, the stiffness of the SMPCs can be distinctly improved by raising the fiber volume fraction.

Here, the thermomechanical behavior and SME of the unidirectional continuous carbon fiber reinforced SMPCs with different φ_0 and v_f will be discussed as follows. As mentioned above, only the SMPCs with

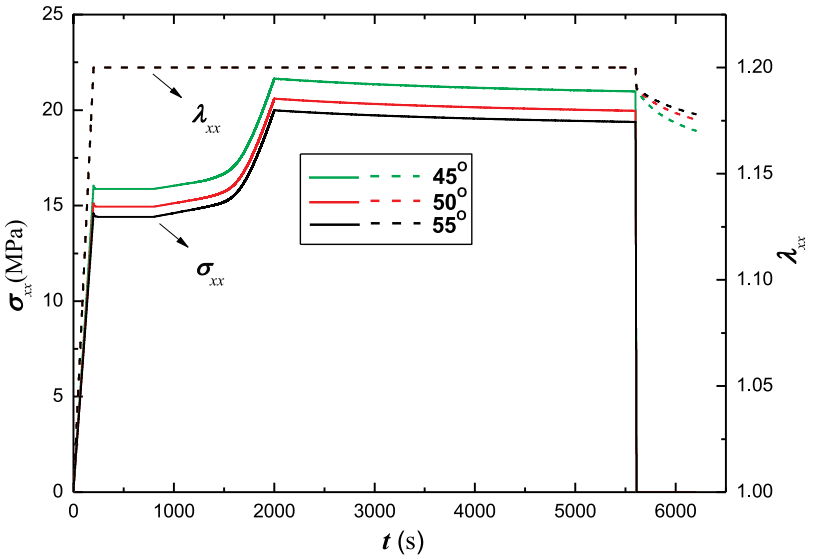

Fig. 12. Simulation results of SMPCs with fiber inclination angles 45°, 50° and 55° for stress and stretch separately as a function of time in the first 3 steps.

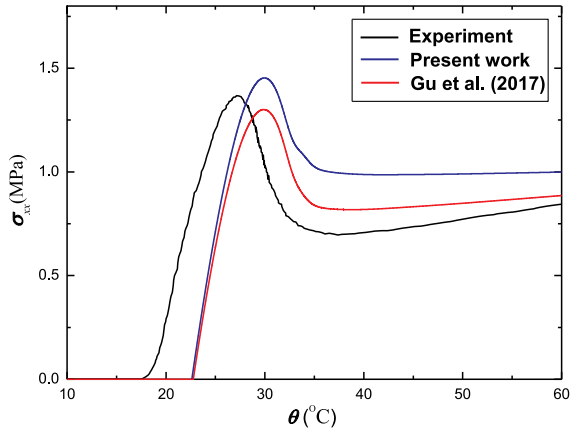

Fig. 13. Comparison of the present work with Gu et al. (2017) for constrained recovery of the SMP.

$43^\circ < \varphi_0 < 58^\circ$ will be studied in order to guarantee the validity of the carbon fiber while the stretch of the SMPC is 1.2. In the simulation, the procedure of a typical thermomechanical shape memory cycle can be divided into 4 steps. Step 1, the lamina is isothermally deformed by applying a longitudinal tensile load at a strain rate of 0.01/s at a temperature well above θ_g (60 °C). Then the lamina is allowed to relax for 10 min to reach thermal equilibration. Step 2, cooling the lamina down to a shape fixing temperature at a rate of 2.5 °C/min while maintaining the deformation constraint. Thereafter, 60 min is given to the lamina for stabilization. Step 3, the deformation constraint is removed at a strain rate of 0.01 /s and the remaining shape is commonly referred to as the temporary shape. At the end of this process, 10 min is given to the specimen for stabilization. Step 4, the SME of the SMPC lamina is activated by raising the temperature to 60 °C at a rate of 2.5 °C/min. Two kinds of recoveries are predicted during this step. The summary simulation conditions is listed in Table 3.

Fig. 11 shows the simulation results of the SMPCs with $\varphi_0 = 45^\circ$ and different v_f for the stress and the stretch separately as a function of time in the first three steps. It can be seen that the stress gradually increases in the cooling process. This should be the reason that the material become stiffer as the temperature decreases. The stress nearly remains the same in the following relaxation process and reaches 0 at the end of the unloading step. During the process of stabilization after unloading, λ_{xx} of the SMPCs with $v_f \geq 0.2\%$ gradually changes as time goes on. The

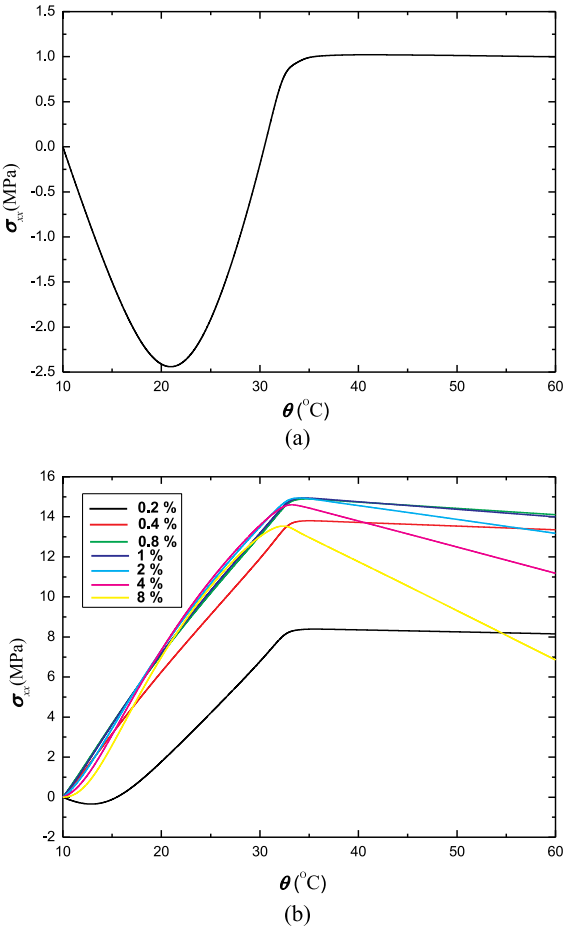

Fig. 14. Recovery stresses of (a) the pure SMP and (b) the SMPCs with different fiber volume fractions.

shape fixity ratio R_{fix} is an important parameter to denote the SME of the SMPCs which can be defined as

$$R_{fix} = \frac{\varepsilon_r}{\varepsilon_p} \times 100\% \tag{40}$$

where ε_p is the initial pre-strain and ε_r is the reserved strain at the end

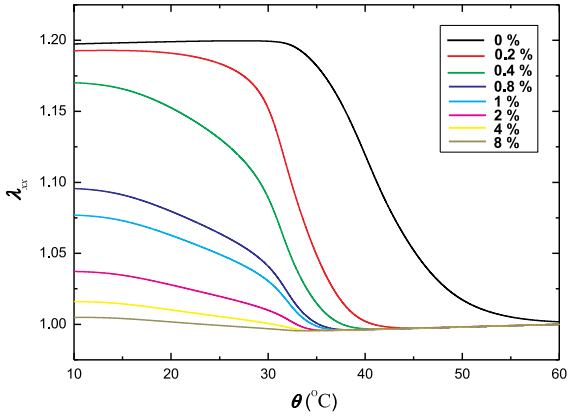

Fig. 15. Recovery stretch of the SMPCs with different fiber volume fractions.

of Step 3 (including the following stabilization process). It is shown that R_{fix} rapidly decreases as v_f increases, for the carbon fiber distinctly improves the stiffness of the SMPCs which causes viscous flow even at a low temperature. Here, the shape fixity ratios of the SMPCs with different fiber volume fractions are listed in Table 4. In order to study the effect of fiber inclination angle on the thermomechanical behavior of the SMPCs, the simulation results of the SMPCs with $v_f = 0.4\%$ and different φ_0 are depicted in Fig. 12. It is found that the carbon fiber with a smaller inclination angle can provide more axial reinforcement, at the expense of the decreasing of shape fixity ratio. It also should be noted that the evolution rule shown in Fig. 12 is accordance with that shown in Fig. 11, due to the reason that both increasing the fiber volume fraction and decreasing the fiber inclination angle can improving the stiffness of the SMPCs. Since the variation of the fiber inclination angle is limited, there is only a little difference between each other. Therefore, the effect of φ_0 on the recovery process will not be studied in this work.

Generally, there are two kinds of recoveries in a typical thermomechanical shape memory cycle, i.e., constrained recovery and free recovery. In the simulation of the constrained recovery, λ_{xx} is kept still and the stress evolution is recorded during heating. It should be noted that the constrained recovery of the pure SMP under compression was explored in the work of Westbrook et al. (2011) and well predicted by Gu et al. (2017). Instead of the eight-chain network model, the hyperelastic constitutive model for fiber reinforced composites is incorporated in this work for the equilibrium component should be the major difference between our model and the model developed by Gu et al. (2017). In order to verify the predictability of the model, a comparison between the simulation result of present work and that of Gu et al. (2017) is shown in Fig. 13. It can be found that the general evolution rule of the stress-temperature response of the model agrees with the experiment and that of Gu et al. (2017) to some extent, which also demonstrate the validity of our model. The prime reason for the discrepancies between the simulation results of both models should be that the stiffness of this model is a little higher than that of the Gu et al. (2017).

The recovery stresses of the pure SMP and the SMPCs with different fiber volume fractions and $\varphi_0 = 45^\circ$ are shown in Fig. 14. It can be found that the viscous flow of the SMP is not triggered in the early stage of the heating process. Therefore, the compressive stress is caused by the thermal expansion. Finally, the tensile recovery stress reaches a steady value after the viscous flow is triggered. It should be noted that this evolution rule of the stress-temperature response for the pure SMP under tension is also in accordance with the experiment carried out by of Liu et al. (2006) (Fig. 16 in this reference). Compared with the recovery stress of the SMPCs, the recovery stress of the pure SMP is small, which is the crucial limitation in its application. It can be found that the peak stress of the SMPCs increases first and then decreases with the increase of fiber volume fraction. The main reason should be that the shape fixity ratio decreases as the fiber volume fraction increases, although the stiffness of the SMPCs increases with the increase of fiber volume fraction. It also can be found that the recovery stress of the SMPC with a higher fiber volume fraction distinctly decreases after reaching the peak stress. This is also mainly caused by the low shape fixity ratio of the SMPCs. Since the reserved tensile strain at the end of Step 3 is rather small, the thermal expansion strain could evidently affect the recovery stress and lead to the stress decrease at the late stage of the heating process.

In the simulation for the free recovery, the sample could deform freely without any constraint and the stretch evolution is recorded during heating. The recovery stretch of the pure SMP and the SMPCs with different fiber volume fractions and $\varphi_0 = 45^\circ$ is shown in Fig. 15. It can be concluded that a higher fiber volume fraction shifts the onset of the stretch recovery to a higher temperature. The prime reason should be that the stiffness of the SMPCs can be greatly improved by the carbon fiber which leads to the viscous flow triggered at a low temperature. From Fig. 15, it also can be found that the SMPCs can rapidly return to their original shape, for the driving stress provided by the carbon fiber is higher than the SMP matrix. Therefore, the recovery time and temperature of SMPCs decrease with the increase of fiber volume fraction.

4. Conclusions

In this paper, a thermoviscoelastic finite deformation constitutive model is developed for thermally activated unidirectional continuous elastic fiber reinforced SMPCs based on thermodynamics with internal state variables. Specifically, the modified Adam-Gibbs model and modified Eying model are separately used to describe the structural relaxation and viscous flow. The hyperelastic constitutive model for transversely isotropic material captures the hyperelastic behavior of the SMPCs up to large deformation at high temperatures. In addition, a CTE model for the transversely isotropic SMPCs is developed here by assuming that the composites are homogenized systems with two phases.

The model developed here shows that the unidirectional continuous carbon fiber reinforced SMPCs with proper fiber inclination angle and volume fraction can be used in finite deformation though the failure tensile strain of carbon fiber is very small (about 2%). This aspect differentiates our model from previous works that mainly focus on the thermomechanical behavior of carbon fiber reinforced SMPCs in the small strain range. Emphasis is laid on the finite deformation thermomechanical response of unidirectional continuous carbon fiber reinforced SMPCs with different fiber inclination angles and fiber volume fractions.

The paper could provide a basis for design and application of unidirectional continuous elastic fiber reinforced SMPCs in engineering. For further study, a series of tests should be carried out to adequately prove the validity and accuracy of the model. It should be noted that there are a great variety of fibers. Classified models should be developed for the specific fiber reinforced SMPCs. At variance with conventional elastic fibers, functional fibers (such as the SMA fiber and crystallizable SMP fiber) can also be used as reinforcements in the SMP matrix to enhance or enable new stimulus approaches and novel SMEs. Therefore, the multi-configuration theory will be used in modeling the thermomechanical finite deformation for these materials in our future work.

Acknowledgments

This work is supported by the National Natural Science Foundation of China (Grant no. 11572153), the Natural Science Foundation of Jiangsu Province of China (BK20170759), a project funded by the Priority Academic Program Development of Jiangsu Higher Education Institutions (PAPD), Outstanding Scientific and Technological

Innovation Team in Colleges and Universities of Jiangsu Province and the Doctor Special Foundation of Nanjing Institute of Technology (ZKJ201603).

References

Boatti, E., Scalet, G., Auricchio, F., 2016. A three-dimensional finite-strain phenomenological model for shape-memory polymers: formulation, numerical simulations, and comparison with experimental data. Int. J. Plasticity 83, 153–177.

Bouaziz, R., Roger, F., Prashantha, K., 2017. Thermo-mechanical modeling of semi-crystalline thermoplastic shape memory polymer under large strain. Smart Mater. Struct. 26 (5), 055009.

Diani, J., Liu, Y., Gall, K., 2006. Finite strain 3D thermoviscoelastic constitutive model for shape memory polymers. Polym. Eng. Sci. 46 (4), 486–492.

Gu, J., Leng, J., Sun, H., 2017. A constitutive model for amorphous shape memory polymers based on thermodynamics with internal state variables. Mech. Mater. 111, 1–14.

Guo, Z.Y., Peng, X.Q., Moran, B., 2007. Mechanical response of neo-Hookean fiber reinforced incompressible nonlinearly elastic solids. Int. J. Solids Struct. 44 (6), 1949–1969.

Ge, Q., Serjouei, A., Qi, H.J., Dunn, M.L., 2016. Thermomechanics of printed anisotropic shape memory elastomeric composites. Int. J. Solids Struct. 102–103, 186–199.

Jarali, C.S., Raja, S., Kiefer, B., 2011. Modeling the effective properties and thermo-mechanical behavior of SMA-SMP multifunctional composite laminates. Polym. Composite 32 (6), 910–927.

Leng, J., Lan, X., Liu, Y., Du, S., 2011. Shape-memory polymers and their composites: stimulus methods and applications. Prog. Mater. Sci. 56 (7), 1077–1135.

Li, G., Wang, A., 2016. Cold, Warm, and hot programming of shape memory polymers. J. Polym. Sci. Pol. Phys. 54 (14), 1319–1339.

Li, Y., He, Y., Liu, Z., 2017. A viscoelastic constitutive model for shape memory polymers based on multiplicative decompositions of the deformation gradient. Int. J. Plasticity 91, 300–317.

Lion, A., Liebl, C., Kolmeder, S., Peters, J., 2010. Representation of the glass-transition in mechanical and thermal properties of glass-forming materials: a three-dimensional theory based on thermodynamics with internal state variables. J. Mech. Phys. Solids 58 (9), 1338–1360.

Liu, Y., Gall, K., Dunn, M.L., Greenberg, A.R., Diani, J., 2006. Thermomechanics of shape memory polymers: uniaxial experiments and constitutive modeling. Int. J. Plasticity 22 (2), 279–313.

Liu, Y., Lv, H., Lan, X., Leng, J., Du, S., 2009. Review of electro-active shape-memory polymer composite. Compos. Sci. Technol. 69 (13), 2064–2068.

Lu, H., Yu, K., Huang, W.M., Leng, J., 2016. On the Takayanagi principle for the shape memory effect and thermomechanical behaviors in polymers with multi-phases. Smart Mater. Struct. 25 (12), 125001.

Mahieux, C.A., Reifsnider, K.L., 2001. Property modeling across transition temperatures in polymers: a robust stiffness-temperature model. Polymer 42 (7), 3281–3291.

Mao, Y., Robertson, J.M., Mu, X., Mather, P.T., Qi, H.J., 2015. Thermoviscoplastic behaviors of anisotropic shape memory elastomeric composites for cold programmed non-affine shape change. J. Mech. Phys. Solids 85, 219–244.

Nguyen, T.D., Qi, H.J., Castro, F., Long, K.N., 2008. A thermoviscoelastic model for amorphous shape memory polymers: incorporating structural and stress relaxation. J. Mech. Phys. Solids 56 (9), 2792–2814.

Nishikawa, M., Wakatsuki, K., Yoshimura, A., Takeda, N., 2012. Effect of fiber arrangement on shape fixity and shape recovery in thermally activated shape memory polymerbased composites. Composites Part A: Applied Science and Manufacturing 43 (1), 165–173.

Qi, H.J., Nguyen, T.D., Castro, F., Yakacki, C.M., Shandas, R., 2008. Finite deformation thermo-mechanical behavior of thermally induced shape memory polymers. J. Mech. Phys. Solids 56 (5), 1730–1751.

Shen, G.L., Hu, G.K., 2006. Mechanics of Composite Materials, first ed. Tsinghua University Press, Beijing.

Song, J.J., Chen, Q., Naguib, H.E., 2015. Constitutive modeling and experimental validation of the thermomechanical response of a shape memory composite containing shape memory alloy fibers and shape memory polymer matrix. J. Intell. Mater. Syst. Struct. 42 (42), 704–718.

Tan, Q., Liu, L., Liu, Y., Leng, J., 2014. Thermal mechanical constitutive model of fiber reinforced shape memory polymer composite: Based on bridging model. Composites Part A: Applied Science and Manufacturing 64, 132–138.

Tool, A.Q., 1946. Relation between inelastic deformability and thermal expansion of glass in its annealing range. J. Am. Ceram. Soc. 29 (9), 240–253.

Westbrook, K.K., Kao, P.H., Castro, F., Ding, Y.F., Qi, H.J., 2011. A 3D finite deformation constitutive model for amorphous shape memory polymers: a multi-branch modeling approach for nonequilibrium relaxation processes. Mech. Mater 43 (12), 853–869.

Xiao, R., Choi, J., Lakhera, N., Yakacki, C.M., Frick, C.P., Nguyen, T.D., 2013. Modeling the glass transition of amorphous networks for shape-memory behavior. J. Mech. Phys. Solids 61 (7), 1612–1635.